

Accepted Article Preview: Published ahead of advance online publication



Generation of polarization-multiplexed terahertz orbital angular momentum combs via all-silicon metasurfaces


Ming-Zhe Chong, Yiwen Zhou, Zong-Kun Zhang, Jin Zhao , Yue-Yi Zhang, Chong-Qi Zhang, Xiaofei Zang, Chao-Hai Du , Pu-Kun Liu and Ming-Yao Xia

Cite this article as: Zhoujie Wu, Haoran Wang, Feifei Chen, Xunren Li, Zhengdong Chen and Qican Zhang. Dynamic 3D shape reconstruction under complex reflection and transmission conditions using multi-scale parallel single-pixel imaging. *Light: Advanced Manufacturing* accepted article preview 10 July, 2024; doi: 10.37188/lam.2024.038

This is a PDF file of an unedited peer-reviewed manuscript that has been accepted for publication. LAM are providing this early version of the manuscript as a service to our customers. The manuscript will undergo copyediting, typesetting and a proof review before it is published in its final form. Please note that during the production process errors may be discovered which could affect the content, and all legal disclaimers apply.

Received: 27 February 2024 Revised: 15 June 2024 Accepted: 29 June 2024
Accepted article preview online 11 July 2024

Generation of polarization-multiplexed terahertz orbital angular momentum combs *via* all-silicon metasurfaces

Ming-Zhe Chong¹, Yiwen Zhou², Zong-Kun Zhang¹, Jin Zhao^{1,3}, Yue-Yi Zhang^{1,3}, Chong-Qi Zhang¹, Xiaofei Zang^{2*}, Chao-Hai Du^{1,3*} , Pu-Kun Liu^{1,3†} and Ming-Yao Xia¹

Abstract

Electromagnetic waves carrying orbital angular momentum (OAM), namely OAM beams, are important in various fields including optics, communications, and quantum information. However, most current schemes can only generate single or several simple OAM modes. Multi-mode OAM beams are rarely seen. This paper proposes a scheme to design metasurfaces that can generate multiple polarization-multiplexed OAM modes with equal intervals and intensities (i.e., OAM combs) working in the terahertz (THz) range. As a proof of concept, we first design a metasurface to generate a pair of polarization-multiplexed OAM combs with arbitrary mode numbers. Furthermore, another metasurface is proposed to realize a pair of polarization-multiplexed OAM combs with arbitrary locations and intervals in the OAM spectrum. Experimental results agree well with full-wave simulations, verifying a great performance of OAM combs generation. Our method may provide a new solution to designing high-capacity THz devices used in multi-mode communication systems.

Keywords: Metasurfaces, Terahertz, Orbital angular momentum comb, Polarization multiplexing

Introduction

Orbital angular momentum (OAM), as an inherent feature of electromagnetic waves (EM waves) with additional degrees of freedom¹, has attracted plenty of interest during the past several decades. The beams carrying OAM, also known as vortex beams or OAM beams, possess vortex wavefront which is defined by topological charge¹. Different OAM modes have different

topological charges. Mathematically, OAM beams with different OAM modes remain orthogonality. So, multi-mode OAM beams can increase channel capacity because of the mode orthogonality². Due to this unique advantage, various applications have emerged, such as super-resolution imaging³, optical trapping⁴, quantum information processing⁵, multi-channel communications^{6,7}, and holography⁸. Currently, enormous methods have been reported to generate OAM beams, including diffractive optical elements⁹, antenna arrays¹⁰, liquid crystals¹¹, and nanosieves³³. However, most reported schemes can only generate single or several simple OAM modes, preventing from flexibly manipulating a series of equally spaced OAM channels with the same intensities, i.e., OAM comb²⁰.

On the other hand, metasurfaces, composed of subwavelength planar microstructures (namely meta-

Correspondence: Xiaofei Zang (xfzang@usst.edu.cn) or Chao-Hai Du (duchaohai@pku.edu.cn)

†Deceased, October 2023.

¹School of Electronics, Peking University, Beijing 100871, China

²Terahertz Technology Innovation Research Institute, and Shanghai Key Lab of Modern Optical System, University of Shanghai for Science and Technology, No. 516 Jun Gong Road, Shanghai 200093, China

Full list of author information is available at the end of the article.

© The Author(s) 2024



Open Access This article is licensed under a Creative Commons Attribution 4.0 International License, which permits use, sharing, adaptation, distribution and reproduction in any medium or format, as long as you give appropriate credit to the original author(s) and the source, provide a link to the Creative Commons license, and indicate if changes were made. The images or other third party material in this article are included in the article's Creative Commons license, unless indicated otherwise in a credit line to the material. If material is not included in the article's Creative Commons license and your intended use is not permitted by statutory regulation or exceeds the permitted use, you will need to obtain permission directly from the copyright holder. To view a copy of this license, visit <http://creativecommons.org/licenses/by/4.0/>.

atoms), are extremely fascinating for their features of compact footprints and strong capabilities to manipulate EM waves¹⁸. By tuning the spacial size of every meta-atom, the phase delay of transmitted (or reflected) EM waves can be flexibly controlled. At the same time, because of the strong anisotropy of meta-atoms, the phase delay usually differs in different incident polarizations¹⁹. In this way, many schemes have been put forward to control surface waves^{12,13,26,28}, generate holograms²⁹⁻³², generate OAM beams^{14,15,22}, manipulate polarization states^{16,17,25,27}, and produce upconversion photoluminescence³⁴. Therefore, metasurfaces are promising candidates for generating polarization-multiplexed wavefront that suits pre-designed functions, including OAM combs. Utilizing metasurfaces, arbitrary polarization-multiplexed OAM combs can be flexibly designed. The OAM combs that contain many orthogonal different OAM modes may be transmitted as a carrier wave in a communication link, such as a wireless THz communication link, providing a promising scheme for an arbitrary multi-mode communication system^{35,36}.

In this paper, we propose, fabricate, and characterize two categories of metasurfaces that can realize the generation of polarization-multiplexed OAM combs working in the terahertz (THz) range. As shown in Fig. 1, the metasurfaces consist of an array of silicon pillars, the sizes of which along the x -direction and y -direction can be independently tuned to produce different propagation phases, thus creating a carefully designed wavefront for both x -polarized and y -polarized (x -pol and y -pol) incident

waves simultaneously. In this way, the modulated wavefront can ultimately form an OAM comb on the focal plane. As a proof of concept, we first design a metasurface to generate a pair of polarization-multiplexed OAM combs with arbitrary lengths, which means that OAM mode numbers within the OAM combs can be arbitrarily controlled. Furthermore, another metasurface is proposed to realize a pair of polarization-multiplexed OAM combs with arbitrarily controlled locations and intervals in the OAM spectrum. Experimental results agree well with full-wave simulations, validating a good performance of OAM combs generation. Our scheme may open a new door to designing high-capacity THz communication devices.

Results

Meta-atoms design

Here, we adopt rectangular silicon pillars and a silicon substrate to construct a transmission-type metasurface, as shown in Fig. 1 and 2a. Each silicon pillar can be regarded as a birefringent scatterer which modulates the complex amplitude of the transmitted EM waves along its long and short axes differently. When the long/short axis is along the x -/ y -direction, its transmissive feature can be described as:

$$\mathbf{T} = \begin{bmatrix} T_{xx} & 0 \\ 0 & T_{yy} \end{bmatrix} \quad (1)$$

where $T_{xx} = t_{xx}e^{i\phi_{xx}}$ and $T_{yy} = t_{yy}e^{i\phi_{yy}}$ are transmission coefficients under x - and y -polarized incidence. Then the

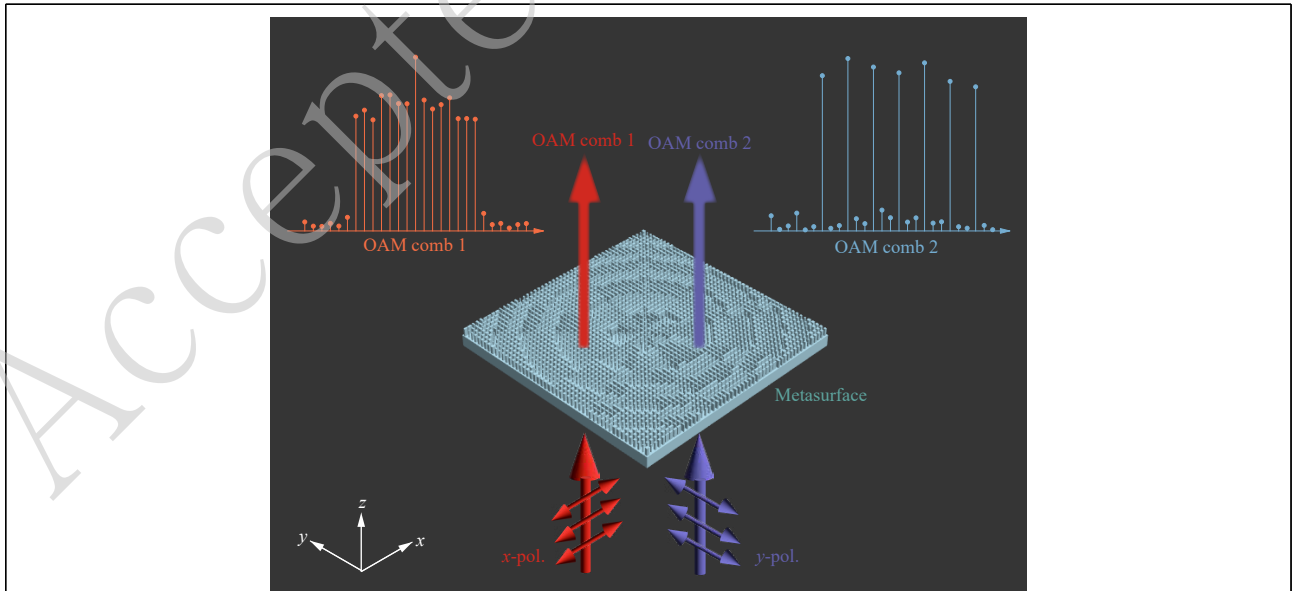
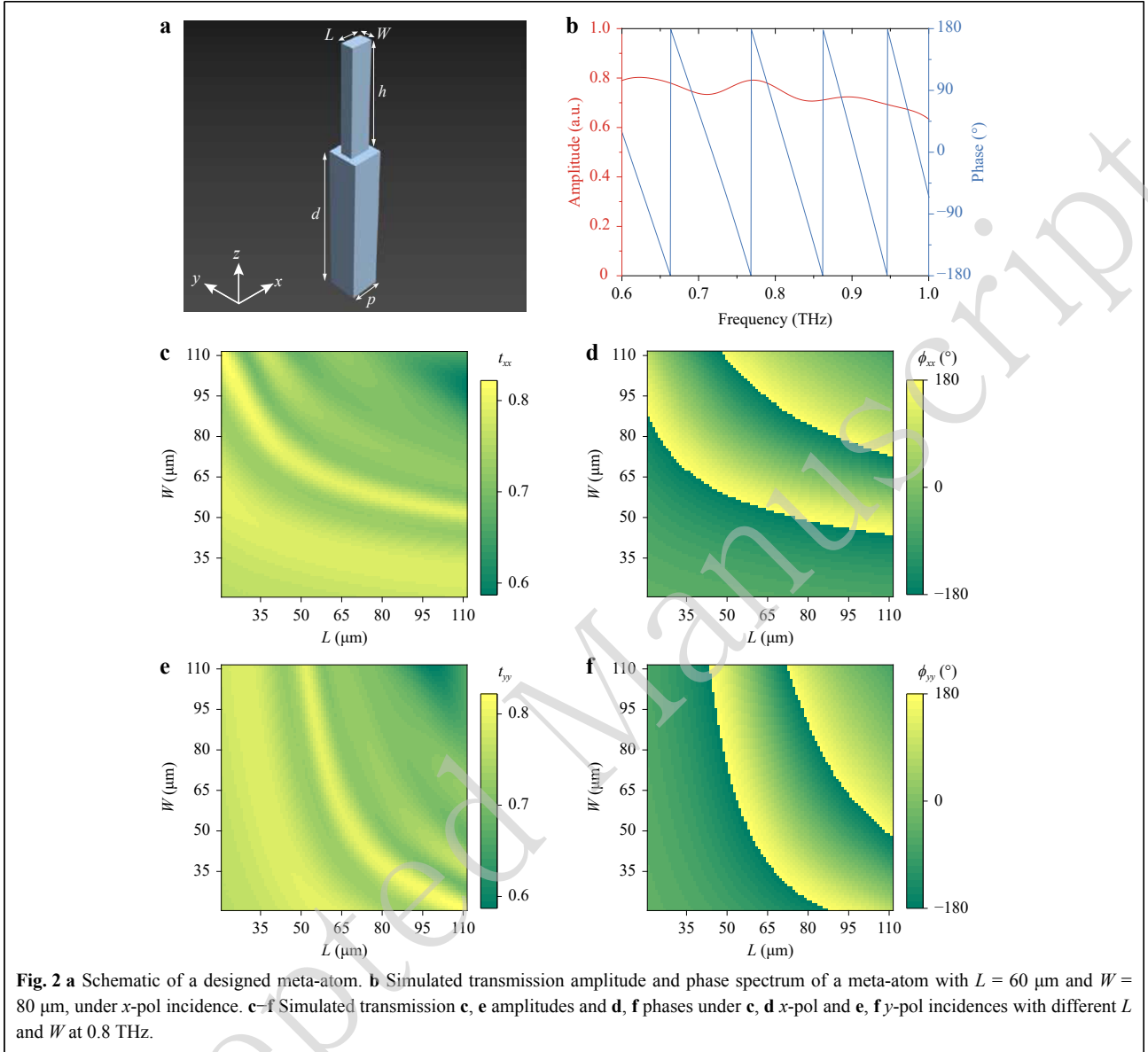


Fig. 1 Schematic of the proposed metasurface for the generation of polarization-multiplexed OAM combs, constructed by silicon pillars as meta-atoms above the silicon substrate. The x -pol and y -pol incident waves normally shine the metasurface and are then converted to OAM comb 1 and 2 on the focal plane, respectively.



transmitted field can be given as:

$$\begin{bmatrix} E_x^{\text{out}} \\ E_y^{\text{out}} \end{bmatrix} = \begin{bmatrix} T_{xx} & 0 \\ 0 & T_{yy} \end{bmatrix} \begin{bmatrix} E_x^{\text{in}} \\ E_y^{\text{in}} \end{bmatrix} = \begin{bmatrix} T_{xx} E_x^{\text{in}} \\ T_{yy} E_y^{\text{in}} \end{bmatrix} \quad (2)$$

where there is no polarization transformation. In this way, the transmitted x - and y -pol fields can be simultaneously modulated by changing the transmissive feature of every meta-atom.

To properly suit the working frequency (0.8 THz), the parameters of meta-atoms are carefully chosen, including period $p = 120 \mu\text{m}$, height $h = 400 \mu\text{m}$, substrate thickness $d = 600 \mu\text{m}$, with length L and width W varying from $20 \mu\text{m}$ to $110 \mu\text{m}$ (see Section A, Supplementary Information). Afterward, we implement full-wave

simulations using the commercial software CST Microwave Studio 2021 (see more details in the Numerical Simulation Section, Methods). A meta-atom's transmission amplitude and phase spectrum with $L = 60 \mu\text{m}$ and $W = 80 \mu\text{m}$ are simulated under x -pol incidence (Fig. 2b), showing a high transmission amplitude from 0.6 THz to 1.0 THz. At the working frequency of 0.8 THz, L and W are swept from $20 \mu\text{m}$ to $110 \mu\text{m}$ to calculate the corresponding transmission amplitudes and phases under x -pol and y -pol incidence, shown in Fig. 2c–f. It can be seen when L and W change, the amplitudes remain high and stable (above 0.6 and below 0.8), while phases cover the whole 360° range for each polarization. In this way, we select 144 meta-atoms with a phase gradient of 30° to

cover the phase range of 0–360° for both x -pol and y -pol incident waves. It is worth noting that the phase gradient of 30° can theoretically provide higher accuracy, while simultaneously satisfying the calculation and fabrication allowance (with more details in Section A, Supplementary Information).

Polarization-multiplexed OAM combs with arbitrary lengths (mode numbers)

To realize the designed function, the meta-atoms need to exhibit the following phase distributions:

$$\begin{cases} \phi_1^x(r, \theta) = \phi_D^x(\theta) + \phi_f(r) \\ \phi_1^y(r, \theta) = \phi_D^y(\theta) + \phi_f(r) \end{cases} \quad (3)$$

Here, (r, θ) is the in-plane position in the polar coordinate system, $\phi_D^x(\theta)$ and $\phi_D^y(\theta)$ represent the Dammann phases for x -pol and y -pol incidences, $\phi_f(r) = -\frac{2\pi}{\lambda}(\sqrt{r^2 + f^2} - f)$ is the focusing phase to converge the transmitted waves ($\lambda = 375 \mu\text{m}$) into the focal plane at focus length $f = 7.5 \text{ mm}$. Traditionally, the Dammann phase is the phase profile for Dammann gratings, a kind of binary optics element, to generate an equal-energy field distribution among all desired diffraction orders²³. In this work, we use the azimuthal Dammann phases to generate OAM combs, while their binary phase values (0 or π) are decided using azimuthal transition points, which can be derived from a numerical optimization method²⁴. These transition points are crucial to generate OAM combs. Then, the transmission coefficient of the first designed azimuthal Dammann phase mask can be described as:

$$T_1(\theta) = \exp(i\phi_D(\theta)) = \sum_{n=-\infty}^{+\infty} C_n \exp(i2\pi n\theta/\Lambda) \quad (4)$$

where Λ is the azimuthal period, and C_n is the coefficient of the n th OAM mode, the value of which can be determined by azimuthal transition points. Thus, modulated by the azimuthal Dammann phase in the θ -space (Fig. 3), OAM combs that contain several OAM series with different topological charges l , are formed after EM waves pass through the metasurfaces. The focusing phase is also added to observe OAM combs on the focal plane. Theoretically, the process of OAM mode analysis can be described by the Fourier transform in the polar coordinate system, and then the OAM spectrum of the field on the focal plane can be written as:

$$E_1(l) = \mathcal{F}\{T_1(\theta)\} = \sum_{n=-\infty}^{+\infty} C_n \delta(l - 2\pi n/\Lambda) \quad (5)$$

where l is the topological charge of an OAM mode, $\mathcal{F}\{\cdot\}$ denotes the Fourier transform, and $\delta(\cdot)$ represents the unit-

impulse function. It is worth noting that l and θ are a pair of Fourier transform bases. In this way, the OAM comb can be realized on the focal plane by selecting a series of transition points, which determine the values of different C_n . To be specific, in Fig. 3a, the transition points are $\theta_n = \{0, 0.23191, 0.42520, 0.52571, 1\} \times 2\pi$ to generate an OAM comb with $l = \{-3, -2, \dots, +3\}$. By contrast, in Fig. 3b, the transition points are $\theta_n = \{0, 0.18240, 0.27424, 0.58581, 0.67967, 0.71917, 0.82217, 0.90642, 1\} \times 2\pi$ to generate an OAM comb with $l = \{-7, -6, \dots, +7\}$. In the two cases, $\Lambda = 2\pi$.

Then we fabricate the first sample through the deep reactive ion etching (DRIE) process (see more details in the Sample Fabrication Section, Methods), the photo of which is demonstrated in Fig. 4a. Sample 1 contains 80×80 rectangular silicon pillars as meta-atoms with a total size of $9.6 \text{ mm} \times 9.6 \text{ mm}$ (with more details in Section B, Supplementary Information). Next, a THz near-field scanning system is adopted to characterize the function of sample 1, as schematically shown in Fig. 4b. The x -pol (or y -pol) incident waves normally shine sample 1, and then the field distributions of the corresponding polarization are detected by a probe on the focal plane with $z = 7.5 \text{ mm}$ (see more details in the Experimental Setup Section, Methods). Fig. 4c, d show the simulated (in the 1st row) and the measured (in the 2nd row) x -pol (or y -pol) electric field distribution of intensity ($|E_x|^2$ or $|E_y|^2$) and phase (ϕ_x or ϕ_y) under x -pol (or y -pol) incidence on the focal plane, suggesting that the simulated results agree with experimentally measured ones. The beams are focused on the central area, where some dark lines suggest an abrupt phase change of π . The field patterns are complicated, indicating there are multi-mode OAM waves (i.e., OAM combs). Theoretically, the electric field distributions on the focal plane (in the polar coordinate system) can be denoted by the superposition of vortex harmonics $\exp(i\theta)$:

$$E(r, \theta) = \frac{1}{\sqrt{2\pi}} \sum_{l=-\infty}^{+\infty} a_l(r) \exp(i\theta) \quad (6)$$

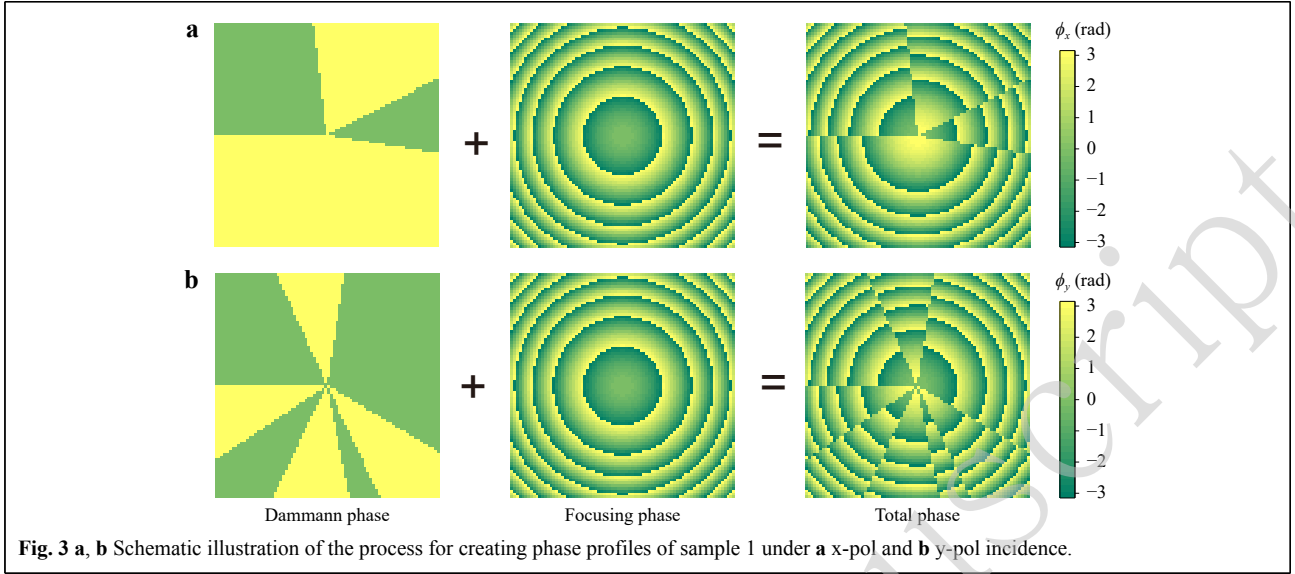
where the complex weights $a_l(r)$ can be calculated by:

$$a_l(r) = \frac{1}{\sqrt{2\pi}} \int_0^{2\pi} E(r, \theta) \exp(-il\theta) d\theta \quad (7)$$

Then the intensity of OAM modes l can be described as:

$$A_l = \int_0^{\infty} |a_l(r)|^2 r dr \quad (8)$$

Using Eq. 7 and 8, We can analyze the simulated and measured field distributions $E(r, \theta)$ at each location (r, θ) in the polar coordinate system. Then the normalized calculated mode intensities $P_l = A_l / \sum_{l=-\infty}^{+\infty} A_l$ under x -pol (or



y-pol) incidence are depicted in Fig. 4e, f. As theoretically predicted, these fields are the superposition of a series of OAM modes with equal intensities (i.e., OAM combs). The x-pol (or y-pol) incident waves passing through sample 1 can be converted to an OAM comb with l from -3 to $+3$ (or from -7 to $+7$), whose length is 7 (or 15). As a result, a pair of polarization-multiplexed OAM combs with different lengths are achieved. The experimental results agree with the simulation. However, there is still some deviation between them. We attribute the causes to the limit of the fabrication and measurement processes, with more details in Section C, Supplementary Information.

Polarization-multiplexed OAM combs with arbitrary locations and intervals

Similarly, the meta-atoms for the second function need to possess the following phase distributions:

$$\begin{cases} \phi_2^x(r, \theta) = \phi_D^x(\theta) + \phi_v^x(\theta) + \phi_f(r) \\ \phi_2^y(r, \theta) = \phi_D^y(\theta) + \phi_v^y(\theta) + \phi_f(r) \end{cases} \quad (9)$$

where $\phi_v^{x,y}(\theta) = l_0^{x,y}\theta$ denotes the vortex phase with a topological charge l_0 for x-pol or y-pol incidence. Specifically, $l_0^x = +3$ and $l_0^y = +2$. Compared with the last section, the vortex phase is added to the total phase distribution. Then the transmission coefficient of the second designed azimuthal phase mask can be written as:

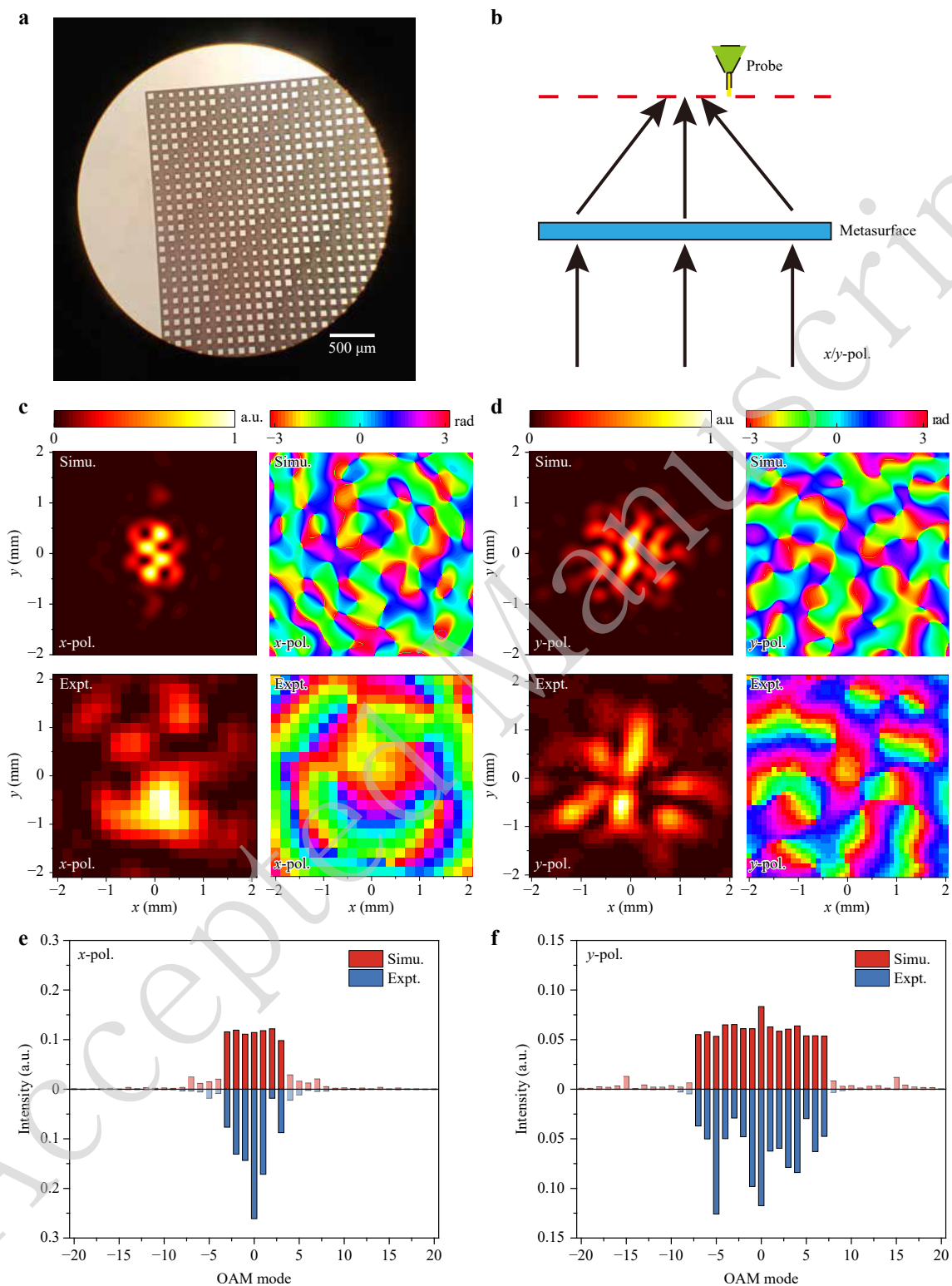
$$\begin{aligned} T_2(\theta) &= \exp(i(\phi_D(\theta) + \phi_v(\theta))) \\ &= \exp(il_0\theta) \sum_{n=-\infty}^{+\infty} C_n \exp(i2\pi n/\Lambda) \end{aligned} \quad (10)$$

After incorporating the focusing phase, on the focal plane, the OAM spectrum of the field can be analyzed by:

$$E_2(l) = \mathcal{F}\{T_2(\theta)\} = \sum_{n=-\infty}^{+\infty} C_n \delta(l - 2\pi n/\Lambda - l_0) \quad (11)$$

In this way, the OAM comb can be formed on the focal plane by selecting l_0 , Λ , and a series of transition points. To be specific, in Fig. 5a, $l_0 = +3$, $\Lambda = \pi$, and the transition points are $\theta_n = \{0, 0.11596, 0.21260, 0.26286, 0.50000, 0.61596, 0.71260, 0.76286, 1\} \times 2\pi$ to generate an OAM comb with $l = \{-3, -1, +1, +3, +5, +7, +9\}$. By contrast, in Fig. 5b, $l_0 = +2$, $\Lambda = 2\pi/3$, and the transition points are $\theta_n = \{0, 0.07730, 0.14173, 0.17524, 0.33333, 0.41064, 0.47507, 0.50857, 0.66667, 0.74397, 0.80840, 0.84190, 1\} \times 2\pi$ to generate an OAM comb with $l = \{-7, -4, -1, +2, +5, +8, +11\}$. It can be easily seen that in the OAM spectrum, the location is l_0 , while the interval is $2\pi/\Lambda$.

We then fabricate the second sample using the DRIE process, the photo of which is shown in Fig. 5e, with the same size as sample 1 (see more details in Section B, Supplementary Information). Next, the function of sample 2 is experimentally measured using the same measurement process shown in the last section. Fig. 5c, d demonstrate the simulated (in the 1st row) and the measured (in the 2nd row) x-pol (or y-pol) electric field distribution of intensity ($|E_x|^2$ or $|E_y|^2$) and phase (ϕ_x or ϕ_y) under x-pol (or y-pol) incidence on the focal plane, suggesting a good agreement between simulated results and experimentally measured ones. After analyzing the field distributions, the normalized calculated mode intensities under x-pol and y-pol incidence are shown in Fig. 5f, g. As theoretically predicted, these fields are OAM combs. The x-pol (or y-pol) incident waves passing through sample 2 can be converted to an OAM comb with $l = \{-3, -1, +1, +3, +5, +7, +9\}$ (or $l = \{-7, -4, -1, +2, +5, +8, +11\}$). Obviously, in the OAM spectrum,



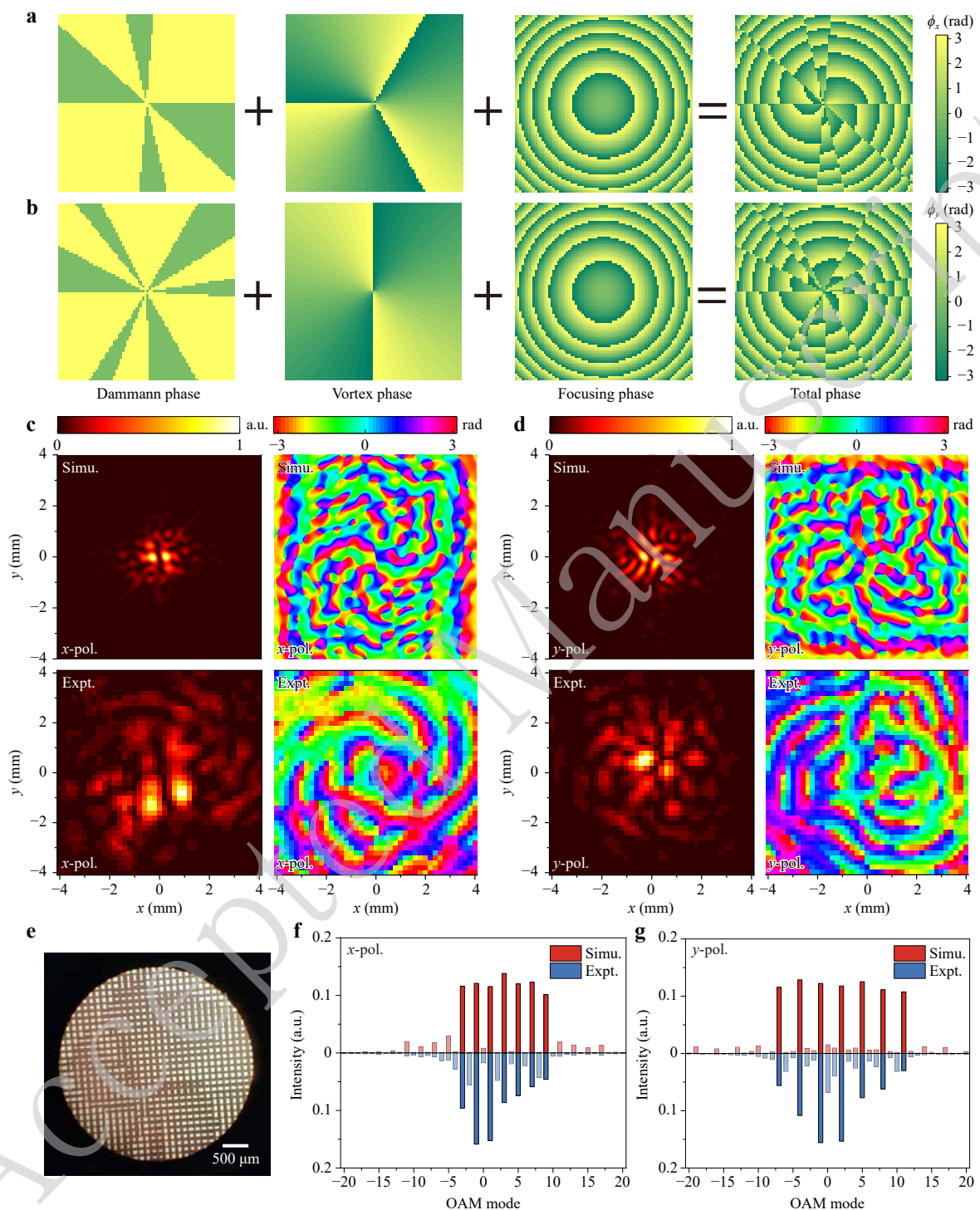


Fig. 5 **a, b** Schematic illustration of the process for creating phase profiles of sample 2 under **a** x -pol and **b** y -pol incidence. **c, d** Simulated (in the 1st row) and measured (in the 2nd row) field distributions of intensity and phase under **c** x -pol and **d** y -pol incidence on the focal plane of sample 2. **e** A photo of part of the fabricated sample 2. **f, g** Calculated OAM spectrum by analyzing simulated and measured field distributions on the focal plane of sample 2 under **f** x -pol and **g** y -pol incidence.

the location of the x -pol (or y -pol) OAM comb is +3 (or +2), while the interval is 2 (or 3). As a result, a pair of

polarization-multiplexed OAM combs with different locations and intervals are achieved. The reasons for the

deviation between measured and simulated results can be found in Section C, Supplementary Information.

Discussion

Some schemes have been reported to realize the generation of OAM combs, but our method has its unique advantage. Compared with the work achieved by shape-tailored metasurfaces¹⁴, our scheme based on the azimuthal Dammann phase can improve the capacity of OAM modes. In addition, compared with the method realized by bulky spatial light modulators (SLMs)²¹, our metasurfaces-based scheme can make the devices more compact, and at least double the theoretical capacity of OAM channels through polarization-multiplexing. Besides, the all-silicon configuration makes the devices easy to fabricate, thus saving the manufacturing cost.

To conclude, we propose a scheme to design metasurfaces that can realize the generation of polarization-multiplexed OAM combs working in the THz range. Utilizing the principle of propagation phases, the wavefront for both x -pol and y -pol incident waves can be manipulated simultaneously, which can ultimately form an OAM comb on the focal plane. As a proof of concept, we first design a metasurface to generate a pair of polarization-multiplexed OAM combs with arbitrary mode numbers. Furthermore, another metasurface is proposed to realize a pair of polarization-multiplexed OAM combs with arbitrary locations and intervals in the OAM spectrum. Experimental results and full-wave simulations are in good agreement, suggesting a great performance of OAM combs generation. Our strategy may provide a new solution to designing high-capacity THz communication devices by introducing multi-mode and dual-polarization configurations.

Materials and methods

Numerical Simulation

All simulations are implemented using the commercial software CST Microwave Studio (version 2021.1). The dielectric constant of silicon is $\epsilon_r = 11.9$. A plane wave (x -pol or y -pol) is defined as the source. The transmission amplitudes and phases of meta-atoms are simulated by the Time Domain Solver. The periodic boundary condition is applied in both the x - and y -directions, while the open boundary condition is utilized in the z -direction. A probe is set 400 μm above the metasurface to detect the transmission coefficient. The sizes of a meta-atom are swept to establish a database of the transmission coefficient, where we select 144 meta-atoms to match the phase gradient of 30° (with more details in Section A, Supplementary Information). Then these meta-atoms are

applied to construct our metasurfaces according to the pre-designed phase profiles. As for the entire metasurfaces, open boundary conditions are applied in the x -, y -, and z -directions. The field distributions can be obtained by setting field monitors at the working frequency.

Sample Fabrication

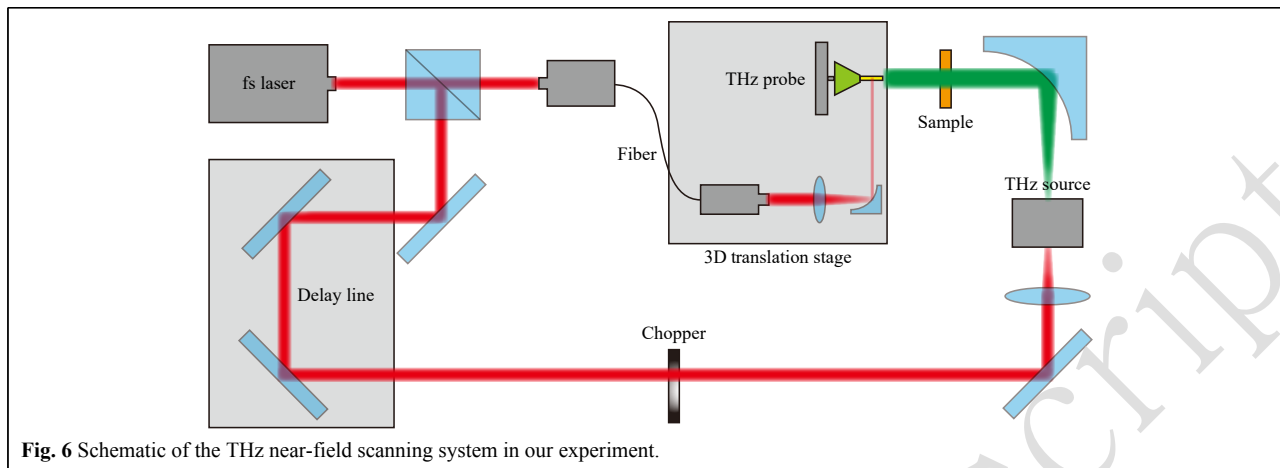
The samples are fabricated using the deep reactive ion etching (DRIE) process (also called as Bosch process). A high-resistance silicon wafer (N-type, $\langle 100 \rangle$) with a thickness of 1 mm and a diameter of 4 inches is chosen as the raw material. First, the wafer is cleaned using the ultrasonic method (with acetone and isopropyl alcohol) for 5 minutes. Next is the lithography process (the machine is SUSS-MA8). The photoresist (AZ4620, with a thickness of about 6.8 μm) is spin-coated (4000 rpm, 30 seconds) on the top of the wafer, which is then baked at 100 $^\circ\text{C}$ for about 150 seconds. Then the wafer is exposed to UV light through a pre-designed mask and then goes through the development process using TMAH developer (25% TMAH; water = 1: 8, 90–120 seconds). Next, the wafer is etched by the DRIE technique (with etching gas of SF_6 and passivation gas of C_4F_8). The etching depth is 400 μm (with an error of ± 20 μm). Then, the photoresist on the wafer is removed using a wet cleaning table (hydrogen peroxide: concentrated sulfuric acid = 1:3). Finally, the wafer is cut to obtain several samples.

Experimental Setup

The measured field distributions are obtained using a THz near-field scanning system based on the terahertz time-domain spectroscopy (THz-TDS) method (shown in Fig. 6). Both the THz source (transmitter) and probe (receiver) are based on the photoconductive antenna technique. The incident femtosecond (fs) laser with a central wavelength of 780 nm is divided into two parts: one part impinges on the THz source to radiate THz waves, while the other part is coupled into a single-mode fiber and then shines the THz probe, which is fixed on a three-dimensional (3D) translation stage to scan the field distributions on the desired plane. After scanning, the field distributions at each location are detected in the time domain. Then performing the Fourier transform, the complex field distributions (including both amplitude and phase) are obtained in the frequency domain. In this way, the amplitude and phase are simultaneously detected at the working frequency (0.8 THz).

Acknowledgements

The authors acknowledge financial support from the National Natural Science Foundation of China (No. 62271011, No. 61971013), and the



National Key Research and Development Program of China (No. 2019YFA0210203).

Author details

¹School of Electronics, Peking University, Beijing 100871, China. ²Terahertz Technology Innovation Research Institute, and Shanghai Key Lab of Modern Optical System, University of Shanghai for Science and Technology, No. 516 Jun Gong Road, Shanghai 200093, China. ³State Key Laboratory of Advanced Optical Communication Systems and Networks, School of Electronics, Peking University, Beijing 100871, China

Data availability

The data supporting the findings of this study are available from the corresponding authors upon reasonable request.

Conflict of interest

The authors declare no competing interests.

Supplementary information is available for this paper at <https://doi.org/10.37188/lam.2024.038>.

Received: 27 February 2024 Revised: 15 June 2024 Accepted: 29 June 2024

References

- Allen, L., Beijersbergen, M. W., Spreeuw, R. J. C. & Woerdman, J. P. Orbital angular momentum of light and the transformation of Laguerre-Gaussian laser modes. *Physical Review A* **45**, 8185-8189 (1992).
- Yao, A. M. & Padgett, M. J. Orbital angular momentum: origins, behavior and applications. *Adv. Opt. Photon.* **3**, 161-204 (2011).
- Liu, K. et al. Super-resolution radar imaging based on experimental OAM beams. *Applied Physics Letters* **110** (2017).
- Ng, J., Lin, Z. & Chan, C. T. Theory of Optical Trapping by an Optical Vortex Beam. *Physical Review Letters* **104**, 103601 (2010).
- Mafu, M. et al. Higher-dimensional orbital-angular-momentum-based quantum key distribution with mutually unbiased bases. *Physical Review A* **88**, 032305 (2013).
- Yan, Y. et al. High-capacity millimetre-wave communications with orbital angular momentum multiplexing. *Nature Communications* **5**, 4876 (2014).
- Bozinovic, N. et al. Terabit-Scale Orbital Angular Momentum Mode Division Multiplexing in Fibers. *Science* **340**, 1545-1548 (2013).
- Fang, X., Ren, H. & Gu, M. Orbital angular momentum holography for high-security encryption. *Nature Photonics* **14**, 102-108 (2020).
- Liu, C. et al. Discrimination of orbital angular momentum modes of the terahertz vortex beam using a diffractive mode transformer. *Opt. Express* **24**, 12534-12541 (2016).
- Kang, L., Li, H., Zhou, J., Zheng, S. & Gao, S. A Mode-Reconfigurable Orbital Angular Momentum Antenna With Simplified Feeding Scheme. *IEEE Transactions on Antennas and Propagation* **67**, 4866-4871 (2019).
- Chen, P. et al. Digitalized Geometric Phases for Parallel Optical Spin and Orbital Angular Momentum Encoding. *ACS Photonics* **4**, 1333-1338 (2017).
- Chong, M. -Z. et al. Spin-decoupled excitation and wavefront shaping of structured surface waves via on-chip terahertz metasurfaces. *Nanoscale* **15**, 4515-4522 (2023).
- Zhang, T. Y. et al. High-Efficiency Metasurface Emitters for Generating Arbitrarily Polarized Spatial Propagating Waves. *Advanced Materials Technologies* **7**, 2200267 (2022).
- Yang, L. -J. , Sun, S. & Sha, W. E. I. Manipulation of Orbital Angular Momentum Spectrum Using Shape-Tailored Metasurfaces. *Advanced Optical Materials* **9**, 2001711 (2021).
- Li, Q. et al. High-Purity Multi-Mode Vortex Beam Generation With Full Complex-Amplitude-Controllable Metasurface. *IEEE Transactions on Antennas and Propagation* **71**, 774-782 (2023).
- Wen, D. et al. Broadband Multichannel Cylindrical Vector Beam Generation by a Single Metasurface. *Laser & Photonics Reviews* **16**, 2200206 (2022).
- Zheng, C. et al. Fine manipulation of terahertz waves via all-silicon metasurfaces with an independent amplitude and phase. *Nanoscale* **13**, 5809-5816 (2021).
- Yu, N. et al. Light Propagation with Phase Discontinuities: Generalized Laws of Reflection and Refraction. *Science* **334**, 333-337 (2011).
- Kats, M. A. et al. Giant birefringence in optical antenna arrays with widely tailorable optical anisotropy. *Proceedings of the National Academy of Sciences* **109**, 12364-12368 (2012).
- Yang, Y. et al. Manipulation of Orbital-Angular-Momentum Spectrum Using Pinhole Plates. *Physical Review Applied* **12**, 064007 (2019).
- Fu, S. et al. Orbital angular momentum comb generation from azimuthal binary phases. *Advanced Photonics Nexus* **1**, 016003 (2022).
- Yuan, Y. et al. Independent phase modulation for quadruplex polarization channels enabled by chirality-assisted geometric-phase metasurfaces. *Nature Communications* **11**, 4186 (2020).
- Dammann, H. & Klotz, E. Coherent Optical Generation and Inspection of Two-dimensional Periodic Structures. *Optica Acta: International Journal of Optics* **24**, 505-515 (1977).

24. Zhou, C. & Liu, L. Numerical study of Dammann array illuminators. *Appl. Opt.* **34**, 5961-5969 (1995).
25. Zheng, C. et al. Creating Longitudinally Varying Vector Vortex Beams with an All-Dielectric Metasurface. *Laser & Photonics Reviews* **16**, 2200236 (2022).
26. Yin, L. -Z. , Zhao, J. , Chong, M. -Z. , Han, F. -Y. & Liu, P. -K. Ultrathin All-Angle Hyperbolic Metasurface Retroreflectors Based on Directed Routing of Canalized Plasmonics. *ACS Applied Materials & Interfaces* **14** (2022).
27. Ke, J. C. et al. Linear and Nonlinear Polarization Syntheses and Their Programmable Controls based on Anisotropic Time-Domain Digital Coding Metasurface. *Small Structures* **2**, 2000060 (2021).
28. Han, J. et al. Tailorable Polarization-Dependent Directional Coupling of Surface Plasmons. *Advanced Functional Materials* **32**, 2111000 (2022).
29. Wu, J. W. et al. Full-State Synthesis of Electromagnetic Fields using High Efficiency Phase-Only Metasurfaces. *Advanced Functional Materials* **30**, 2004144 (2020).
30. Chen, K. et al. Directional Janus Metasurface. *Advanced Materials* **32**, 1906352 (2020).
31. Li, L. et al. Electromagnetic reprogrammable coding-metasurface holograms. *Nature Communications* **8**, 197 (2017).
32. Wei, M. et al. Extended Metasurface Spin Functionalities from Rotation of Elements. *Advanced Optical Materials* **10**, 2201975 (2022).
33. Jin, Z. et al. Phyllotaxis-inspired nanosieves with multiplexed orbital angular momentum. *eLight* **1**, 5 (2021).
34. Feng, Z. et al. Dual-band polarized upconversion photoluminescence enhanced by resonant dielectric metasurfaces. *eLight* **3**, 21 (2023).
35. Yuan, S. S. A. et al. Approaching the Fundamental Limit of Orbital-Angular-Momentum Multiplexing Through a Hologram Metasurface. *Physical Review Applied* **16**, 064042 (2021).
36. Zhou, H. et al. Utilizing multiplexing of structured THz beams carrying orbital-angular-momentum for high-capacity communications. *Opt. Express* **30**, 25418-25432 (2022).